Eur. Phys. J. D (2022) 76:79
https://doi.org/10.1140/epjd/s10053-022-00392-9

THE EUROPEAN PHYSICAL JOURNAL D

Topical Review - Atomic and Molecular Collisions

Photofragmentation dynamics study of $ArBr_2$ $(v = 16, \ldots, 25)$ using two theoretical methods: trajectory surface hopping and quasiclassical trajectories

Ernesto García-Alfonso[1,2], Maykel Márquez-Mijares[1], Jesús Rubayo-Soneira[1,a], Nadine Halberstadt[2], KennethC. Janda[3], and CraigC. Martens[3]

[1] Instituto Superior de Tecnologías y Ciencias Aplicadas (InSTEC), Universidad de La Habana, Ave. Salvador Allende 1110,Plaza de la Revolución, Habana 10400, Cuba
[2] Université Toulouse 3 and CNRS Laboratoire des Collisions Agrégats et Réactivité IRSAMC, 118 Route de Narbonne, F-31062 Toulouse, Cedex 09, France
[3] Department of Chemistry, University of California, Irvine, CA 92697-2025, USA

Received 23 December 2021 / Accepted 23 March 2022 / Published online 6 May 2022

Abstract. The vibrational predissociation of van der Waals complexes has been the object of study using a wide range of theoretical and experimental methods, producing a large number of results. We focus here on the $ArBr_2$ $(v = 16, \ldots, 25)$ system. For its study, we employ two important theoretical methods: the trajectory surface hopping (TSH) and the quasiclassical trajectory method (QCTM). In the first case, the dynamics of the system are reproduced on a potential energy surface (PES) corresponding to quantum molecular vibrational states. The possibility of hopping to other vibrational surfaces is also included, which can then lead to van der Waals bond dissociation. On the other hand, the second case consists of propagating the dynamics over a single potential energy surface. We incorporate the kinetic mechanism into the TSH method for better comparison of the evolution of the complex. Both methods allow us to study the dynamical behavior of the $ArBr_2$ as well as several observables. We compute the lifetime, exit channel, rotational energy, and maximum angular momentum (j_{max}) of Br_2. We compare our results with previous experimental and theoretical work and also report new results for cases that have not previously been considered.

1 Introduction

The noble gas halogen van der Waals (vdW) molecules, where weakly bound rare gas atoms are interacting with a strong chemical bond like Br_2, are considered ideal systems to study molecular energy transfer mechanisms and how molecular properties influence intramolecular dynamics. Due to the weakness of the vdW interactions, it is expected that the remaining constituents in these kinds of complexes retain their chemical properties so the energy transfer mechanisms can be easily identified and studied at the state-to-state level. From the experimental point of view, the spectroscopy of these molecules is available as well as real-time dynamics on femtosecond to picosecond time scales. There are a variety of theoretical models which may be formulated and tested with the experimental results [1–19].

The quasiclassical trajectory method is one of the more popular approaches to study the molecular dynamics of these systems. This formulation solves the classical equations of motion using initial conditions generated from quantum probabilities distributions. It exhibits substantially lower computational costs compared with exact quantum methods. The quasiclassical approach allows the construction of intuitive models for molecular processes. In some cases, the full dimensionality of the system can be included.

The $ArBr_2$ complex has been the subject of previous experimental and theoretical work [20–23]. Dissociation rates have been determined for $v = 16 - 25$ of the B electronic state. The results showed that, while the rate generally increases with vibrational quantum number, the trend is not monotonic, suggesting that $ArBr_2$ undergoes vibrational predissociation (VP) in the sparse intramolecular vibrational distribution (IVR) regime. This was confirmed by a theoretical analysis of the fragmentation dynamics [21], which was able to qualitatively reproduce the experimental results. So far, no more global studies have been done on this system, so it is of interest to implement the QCTM scheme to investigate other criteria of the processes exhibited by this complex.

Supplementary Information The online version contains supplementary material available at https://doi.org/10.1140/epjd/s10053-022-00392-9.

[a] e-mail: jrubayo@gmail.com (corresponding author)

The trajectory surface hopping method (TSH) [24] has demonstrated its validity and efficiency for a variety of molecular dynamics problems [13,15–17,25–29].

For the study of $ArBr_2$, we have used a diabatic representation in which the potential energy surfaces are formed by the interaction of the Ar atom with the vibrational levels ($v = 16, 17, \ldots, 25$) of Br_2. To understand the evolution of the system, we have implemented a kinetic mechanism recently used for $NeBr_2$ vibrational predissociation [25] and inspired by earlier work [13,17,18]. In this work, the transfer of up to five vibrational quanta is included in the kinetic mechanism.

2 Theory and methodology

The photodissociation process of interest in this work is described as:

$$\begin{aligned} &ArBr_2(X, v = 0) + \hbar\omega \rightarrow [ArBr_2(B, v' = 16 - 25)] \\ &\overset{VP}{\rightarrow} Ar + Br_2(B, v'') \end{aligned}$$

Two different approaches are used in our simulations: quasiclassical trajectory and trajectory surface hopping in the diabatic representation. Our results have been compared to existing experimental and wave packet results.

We employ Jacobi coordinates (r, R, θ) which are widely used for this kind of molecular geometry. The coordinate r is the bond length of Br_2, and R is the intermolecular distance from the center of mass of the dihalogen to the Ar atom. The angle θ is defined by the $\mathbf{r}$ and $\mathbf{R}$ vectors. These definitions are illustrated in Fig. 1. In our calculations, we take the total angular momentum to be zero ($\mathbf{J} = \mathbf{j} + \mathbf{l} = \mathbf{0}$), with $\mathbf{j}$ being the angular momentum of Br_2 (associated with $\mathbf{r}$) and $\mathbf{l}$ the orbital angular momentum (associated with $\mathbf{R}$), which is a justified constraint for studying photodissociation events occurring at low temperature [6]. The classical Hamilton function corresponding to this three-degree-of-freedom model of the complex is written as

$$\begin{aligned} H(r, R, \theta) = H_{Br_2} + \frac{1}{2\mu_{ArBr_2}}\left(p_R^2 + \frac{p_\theta^2}{R^2}\right) \\ + V_{ArBr_2}(r, R, \theta), \end{aligned} \tag{1}$$

where H_{Br_2} is the diatomic Hamiltonian

$$H_{Br_2} = \frac{1}{2\mu_{Br_2}}\left(p_r^2 + \frac{p_\theta^2}{r^2}\right) + V_{Br_2}(r), \tag{2}$$

In the equations above, p_r, p_R, and p_θ are the momenta associated with coordinates r, R, and θ, respectively; μ_{Br_2} and μ_{ArBr2} stand for the reduced masses for r (Br_2) and R ($ArBr_2$), respectively ($\mu_{Br_2}^{-1} = m_{Br}^{-1} + m_{Br}^{-1}$ and $\mu_{ArBr_2}^{-1} = m_{Ar}^{-1} + (m_{Br} + m_{Br})^{-1}$).

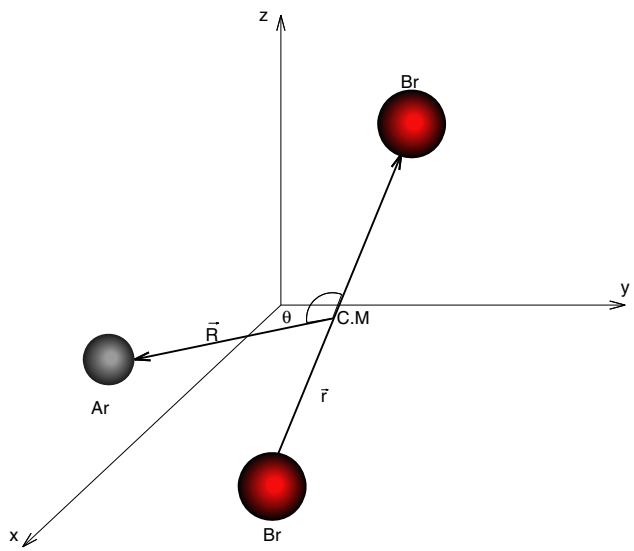

Fig. 1 Jacobi coordinates for Ar...Br_2

Both Br–Br (V_{Br_2}) and Ar–Br (V_{ArBr}) interactions are represented as a Morse potential:

$$V_{AB}(x) = D(e^{-2\alpha(x-\bar{x})} - 2e^{-\alpha(x-\bar{x})}), \tag{3}$$

where $\bar{x}$ is the equilibrium position. Van der Waals interaction is constructed by the pairwise sum of two Morse potential (atom-atom interactions)

$$V_{ArBr2}(r, R, \theta) = V_{ArBr}(R_1) + V_{ArBr}(R_2), \tag{4}$$

with

$$R_{1,2}^2 = R^2 + (r/2)^2 \pm rR\cos(\theta),$$

The interaction potential Br–Br was taken from Ref. [31] which it was obtained adjusting a Morse potential to RKR potential reported in Ref. [30]. It reproduces very well our region of interest, from $v = 16$ to $v = 25$. The potential parameters are collected in Table 1.

2.1 Quasiclassical trajectory method

The basis of the quasiclassical methodology is to solve the classical equations of Hamilton once the initial state of the system is determined. In particular, our variant of the QCTM is based on the idea that the best trajectory ensemble representation of the initial state is provided by the corresponding quantum distribution function.

We follow here a procedure similar to that used in Ref.[6] for $NeBr_2$ vibrational predissociation. We recall here its essential features, adapted to the present study.

We have chosen a sampling of both the initial configurations and the conjugate momenta. After running many trajectories, statistical analysis is used to compute observables from the details of the ensemble of trajectories.

Table 1 Morse potential parameters

Interaction	D (cm^{-1})	α ($Å^{-1}$)	$\bar{R}$ (Å)
Br–Br	3788	2.045	2.667
Ar–Br	114	1.80	4.10

Initial conditions representing a microcanonical distribution for the system are obtained by solving the time-independent Schrödinger equation for the quasi-bound state in the vibrational level v of the B electronic state, sampling the coordinates following the resulting probability density and deducing the momenta to obtain the bound state energy. The Hamiltonian operator corresponding to the B state is

$$H(r,R,\theta)\,|\Omega_v^B(r,R,\theta)\rangle = E\,|\Omega_v^B(r,R,\theta)\rangle. \quad (5)$$

Here, H is the quantum Hamiltonian operator for the system corresponding to $J=0$ [Eq. (1)]. A diabatic representation $|\Omega_v^B(r,R,\theta)\rangle = |\psi_v^B(r)\rangle\,|\Phi_v^B(R,\theta)\rangle$ is employed.

The relevant diatomic wavefunctions $|\psi_v^B(r)\rangle$ and energies $E^{B,v}_{Br_2}$ are obtained from

$$[H^B_{Br_2} - E^{B,v}_{Br_2}]\,|\psi_v^B(r)\rangle = 0 \quad (6)$$

and taking into account $p_\theta = 0$.

The state $|\Phi_v^B(R,\theta)\rangle$ is calculated by solving Eq. 7 using the Truhlar–Numerov method. We fixed $\theta = \pi/2$, for which the system is more bound. This corresponds to a "T" shape configuration. We have also taken $r = \bar{R}$ for the Br–Br and $j = 0$. The initial rotational quantum number for the Br_2 molecule can be neglected ($j = 0$), as we will see in the results, because the anisotropy effect is not very strong in this system. Vibrational energies for Br–Br and $ArBr_2$ are collected in Table 2.

$$\frac{1}{2\mu_{ArBr_2}}\left(-\hbar^2\frac{\partial^2}{\partial R^2} + \frac{\hat{j}^2}{R^2}\right)|\Phi_v^B(R,\theta)\rangle + \left[\langle\psi_v^B|\,V_{ArBr_2}(r,R,\theta)|\psi_v^B\rangle - (E^B - E^{B,v}_{Br_2})\right] |\Phi_v^B(R,\theta)\rangle = 0 \quad (7)$$

Once the initial configurations are determined to statistically reproduce the quantum distributions, the conjugate momenta p_r and p_R are obtained from energy conservation as in Ref.[6].

Hamilton's equations, given for $H^{J=0} = H(r,R,\theta)$,

$$\frac{dr}{dt} = \frac{\partial}{\partial p_r}[H^{J=0}] = \frac{p_r}{\mu_{Br_2}} \quad (8)$$

$$\frac{dR}{dt} = \frac{\partial}{\partial p_R}[H^{J=0}] = \frac{p_R}{\mu_{ArBr_2}} \quad (9)$$

$$\frac{d\theta}{dt} = -\frac{\partial}{\partial p_\theta}[H^{J=0}] = p_\theta\left(\frac{1}{\mu_{Br_2}r^2} + \frac{1}{\mu_{ArBr_2}R^2}\right) \quad (10)$$

Table 2 v are the vibrational levels for isolated Br–Br

v	E_v (cm^{-1})	E_v^{vdW} (cm^{-1})
16	−1570.98	−202.77
17	−1467.53	−202.55
18	−1367.61	−202.32
19	−1271.21	−202.06
20	−1178.34	−201.79
21	−1088.99	−201.49
22	−1003.17	−201.17
23	−920.88	−200.83
24	−842.11	−200.43
25	−766.86	−200.04

E_v are the energies for those vibrational levels and E_v^{vdW} represents the ground energy for $\langle v|\,V_{ArBr_2}(r,R,\theta)|v\rangle$

$$\frac{dp_r}{dt} = -\frac{\partial}{\partial r}[H^{J=0}] = \frac{p_\theta^2}{\mu_{Br_2}r^3} - \frac{\partial}{\partial r}\left[V_{Br_2}(r) + V_{ArBr_2}(r,R,\theta)\right] \quad (11)$$

$$\frac{dp_R}{dt} = -\frac{\partial}{\partial R}[H^{J=0}] = \frac{p_\theta^2}{\mu_{ArBr_2}R^3} - \frac{\partial}{\partial R}[V_{ArBr_2}(r,R,\theta)] \quad (12)$$

$$\frac{dp_\theta}{dt} = -\frac{\partial}{\partial \theta}[H^{J=0}] = -\frac{\partial}{\partial \theta}[V_{ArBr_2}(r,R,\theta)] \quad (13)$$

are numerically integrated by using a fourth-order Adams–Moulton algorithm initiated by a fourth-order Runge–Kutta integrator. The time step is $\Delta t = 0.1$ fs. Total energy conservation of $\Delta E < 10^{-8}$ cm^{-1} is achieved. Propagation is terminated if any of the following conditions are satisfied: $t > 600$ ps or $R > 10$ Å, the former corresponding to $6{\cdot}10^6$ maximum integration cycles and the latter assumed to correspond to a dissociated trajectory since the vdW interaction becomes negligible at that distance. The total number of trajectories in the ensemble is $N = 5{\cdot}10^3$ for each $v = 16-25$.

To obtain quantum numbers from classical statistics, the so-called standard binning procedure is used [6].

2.2 TSH method in the diabatic representation

The TSH approach for treating vibrational predissociation in this diatomic-rare gas atom system follows the same idea as earlier work [15–18] and is described in detail in Ref.[25]. We recall here its essential features. The diatomic vibrational coordinate (r) is treated as a quantum coordinate while the other degrees of freedom R and θ are treated as classical coordinates. The Hamiltonian for the system can be written as:

$$H(r,R,\theta) = H_q(r) + H_{cl}(R) + H_{int}(r,R,\theta) \quad (14)$$

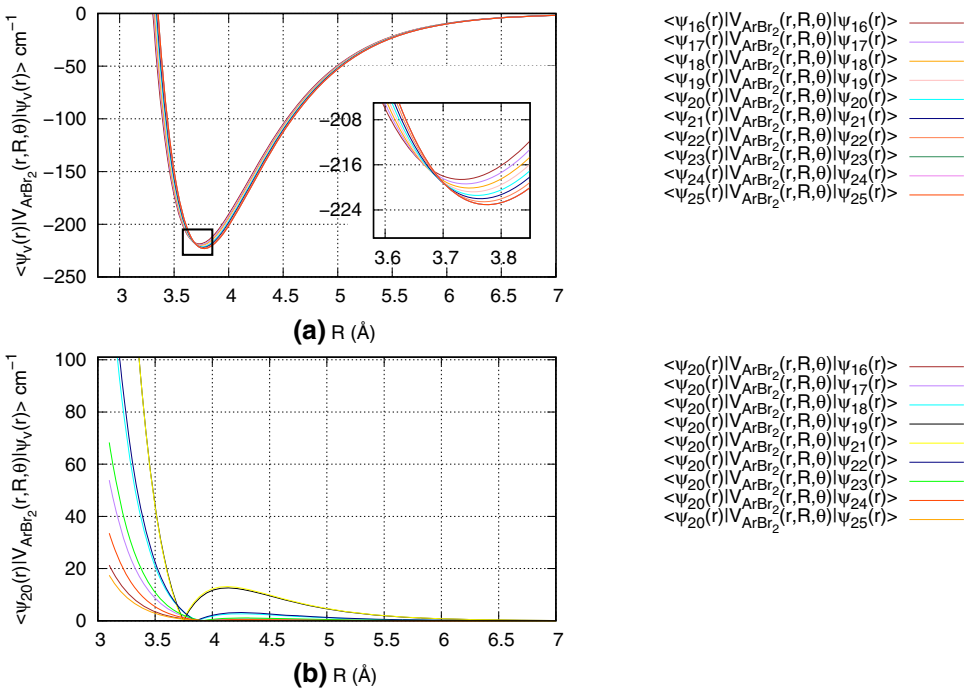

Fig. 2 Van der Waals interactions and couplings for Ar-Br_2 vibrational predissociation. **a** Diagonal $\langle\psi_v^B(r)|\, V_{\mathrm{ArBr_2}}(r,R,\theta)|\psi_v^B(r)\rangle$ matrix elements defining the v^{th} surface for TSH classical coordinates R and θ; **b** Off-diagonal matrix elements $|\langle\psi_{20}^B(r)|\, V_{\mathrm{ArBr_2}}(r,R,\theta)|\psi_v^B(r)\rangle|$ between v=20 and different vibrational levels as a function of the Ar to Br_2 distance R, defining the coupling responsible for VP of v=20. Note that the absolute value of the coupling is represented in order to stress the importance of the repulsive region of the potential; the coupling itself changes sign near R=3.87 Å. All curves are calculated for the "T" shape configuration ($\theta = 90°$)

where the quantum Hamiltonian describes Br_2 vibration

$$H_q(r) = -\frac{\hbar^2}{2\mu_{Br_2}}\frac{\partial^2}{\partial r^2} + V_{\mathrm{Br_2}}(r) \tag{15}$$

the classical Hamiltonian describes the intermolecular degrees of freedom

$$H_{cl}(R) = \frac{p_R^2}{2\mu_{\mathrm{ArBr_2}}} + \frac{p_\theta^2}{2\mu_{\mathrm{ArBr_2}}R^2} \tag{16}$$

and the coupling between the quantum and classical degrees of freedom is

$$H_{int}(r,R,\theta) = \frac{p_\theta^2}{2\mu_{\mathrm{Br_2}}r^2} + V_{\mathrm{ArBr_2}}(r,R,\theta). \tag{17}$$

Defining $|v\rangle \equiv |\psi_v^B(r)\rangle$ to simplify notation, the Hamiltonian matrix elements can be written as

$$\begin{aligned}\langle v'|\, H(r,R,\theta)|v\rangle = {} & \langle v'|\, V_{\mathrm{ArBr_2}}(r,R,\theta)|v\rangle \\ & + \frac{p_\theta^2}{2\mu_{\mathrm{Br_2}}}\langle v'|\,\frac{1}{r^2}|v\rangle \\ & + \left(\frac{p_\theta^2}{2\mu_{\mathrm{ArBr_2}}R^2} + E_{\mathrm{Br_2}}^{B,v} \right. \\ & \left. + \frac{p_R^2}{2\mu_{\mathrm{ArBr_2}}}\right)\delta_{vv'},\end{aligned}$$

where $\delta_{vv'}$ is the Kronecker's delta and $E_{\mathrm{Br_2}}^{B,v}$ is the vibrational energy for Br_2 obtained in Eq. (6).

The classical equations of motion on the v^{th} surface are then the same ones as Eqs. (9), (10), (12), and (13), replacing $H^{J=0}$ with $\langle v|\, H^{J=0}|v\rangle$ and $\frac{1}{r^2}$ with $\langle v|\,\frac{1}{r^2}|v\rangle$ [16,25]. The PES are generated by $\langle v|\, H^{J=0}|v\rangle$ and the couplings by $\langle v'|\, H^{J=0}|v\rangle$ with $v' \neq v$, see Fig. 2a, b.

The state vector $|\Psi(t)\rangle$ describing the vibration of Br_2 as a function of time-dependent Schrödinger equation at the current value of the classical coordinates is

$$i\hbar\frac{\partial|\Psi(t)\rangle}{\partial t} = [H_q(r) + H_{int}(r,R,\theta)]\,|\Psi(t)\rangle. \tag{18}$$

The evolving state $|\Psi(t)\rangle$ is expanded as

$$|\Psi(t)\rangle = \sum_v c_v(t)e^{-iE_{\mathrm{Br_2}}^{B,v}\,t/\hbar}|v\rangle \tag{19}$$

The c_v are propagated using the same numerical integrator algorithm as above.

The time-dependent population of each vibrational level is determined as follows:

$$\rho_{vv'}(t) = c_v(t)c^*_{v'}(t), \tag{20}$$

where $\rho_{vv'}(t)$ is the density matrix.

The transition probabilities, following the Tully's procedure [24], from the current state v to all other states $v' \neq v$ during the time interval Δt are computed using the surface hopping probabilities Eq. (21).

$$g_{v\to v'} = \frac{2\Delta t}{\hbar}\frac{Im\left(c^*_v(t)c_{v'}(t)e^{[i(E^{B,v}_{Br_2}-E^{B,v'}_{Br_2})t/\hbar]}\right)}{|c_v(t)|^2} \langle v'|\, H_{int}(r,R,\theta)|v\rangle. \tag{21}$$

The initial conditions for the classical trajectories are selected randomly as in the QCTM method, for a total energy corresponding to the zero-point of the complex $ArBr_2$, for a particular vibrational state of the Br_2 molecule.

When state jumps occur, classical momenta are adjusted in order to conserve the total energy [15,36]. In our case, quantum jumps (vibrational transitions) occur between diabatic surfaces, defined for each vibrational level and coupled by the $ArBr_2$ potential. The classical linear momentum vectors p_R and p_θ are adjusted after a surface hop to compensate the difference in potential energy, the analogous way as in Ref. [25].

When a hop to a higher vibrational level is attempted, it can be frustrated, *i.e.,* the energy conservation equation does not have a real solution.

We then applied the fewest switches with time uncertainty (FSTU) method of Ref. [37], which can be interpreted as the ability of a quantum system to borrow energy ΔE for a time Δt given by the uncertainty principle. This feature allows the trajectory $R(t)$ that experiences a frustrated hop to tunnel and hop successfully at some nearby geometry along $R(t)$ within the time interval Δt.

If FSTU does not avoid the frustrating hop, we then apply the "∇V" prescription Ref. [38]. That allows us change the sign or not of the linear momentum. We have to take into account the influence of the target PES on the particle. If both the nuclear momentum and the force have the same direction, the particle does not feel the force and therefore it does not affect its motion. In the other case, the direction is affected.

In addition, when a hop occurs, we reset the wave function employing the "instantaneous decoherence" (ID) approach [36]

- $c_v = 0 \;\forall\; v \neq v'$
- $c_{v'} = 1$

2.3 Kinetic mechanism

In order to gain insight into the energy relaxation paths followed by the system, we fit the $Br_2(v-i)\cdots$ Ar and $Br_2(v-i)$ populations resulting from the TSH simulation to a kinetic mechanism introduced by Miguel [13] (see supplementary material). This mechanism is based on three types of elementary steps: vibrational predissociation (VP), where the transfer of one vibrational quantum from the diatomic to the Van der Waals degrees of freedom dissociates the complex; intramolecular vibrational relaxation, where one vibrational quantum is transferred but no dissociation occurs; and evaporative cooling (EC) when enough energy has been collected in the intermolecular modes and the Ar atom dissociates without transfer of a new vibrational quantum.

In the case of $Ar\cdots Br_2$, the transfer of one vibrational quantum of Br_2 to the vdW modes is not sufficient to dissociate the complex. Hence, it is an IVR step which leads to an intermediate complex, denoted by $Br_2(v-1)\cdots\ Ar_{ivr}$, with excited intermolecular modes. The second quantum transfered can go either to the dissociative mode (VP step, if Δv=-2 is open), leading to $Br_2(v-2)\cdots\ Ar_{vp}$ which quickly dissociates to $Br_2(v-2)$ + Ar, or add up to the van der Waals mode excitation (IVR), leading to $Br_2(v-2)\cdots\ Ar_{ivr}$. The same processes can be iterated for the loss of up to five quanta. When enough energy has been collected in the intermolecular modes, the complex can dissociate at the same Br_2 vibrational level via evaporative cooling (EC).

The $Br_2(v-i)\cdots$ Ar populations detected in the TSH simulation are thus the sum of two contributions: a short-lived one coming from the VP process, $Br_2(v-i)\cdots\ Ar_{vp}$, and a longer-lived one coming from the IVR process, $Br_2(v-i)\cdots\ Ar_{ivr}$. Depending on the nature of the last step, *i.e.,* the step leading to dissociation, the mechanism is labeled as IVR-VP or IVR-EC.

3 Results

3.1 Vibrational predissociation lifetimes

We have computed the lifetime for QCTM taken as the sum of two different exponential decay laws, Eqs. (22) and (23), where N_{NDT} stands for non-dissociated trajectories and N_T the total number of trajectories [6].

$$\frac{N_{NDT}(t)}{N_T} \sim (\alpha_1 e^{-\alpha_2 t} - \alpha_2 e^{-\alpha_1 t})\alpha_1 > \alpha_2 \tag{22}$$

$$\frac{N_{NDT}(t)}{N_T} \sim \alpha_1 e^{-\alpha_2 t}. \tag{23}$$

The parameter α_2 is related with the lifetime (τ) by the equation $\tau = \alpha_2^{-1}$, while α_1^{-1} is associated mainly with the IVR processes among other factors influence [6]. The parameter α_1 takes into account the initial slow decay due to the use of classical dynamics [6]. Figure 3 displays the QCTM dissociation times for $v = 23$ using Eq. (22) or (23) . For $t \leq 2$ ps the system is still bound

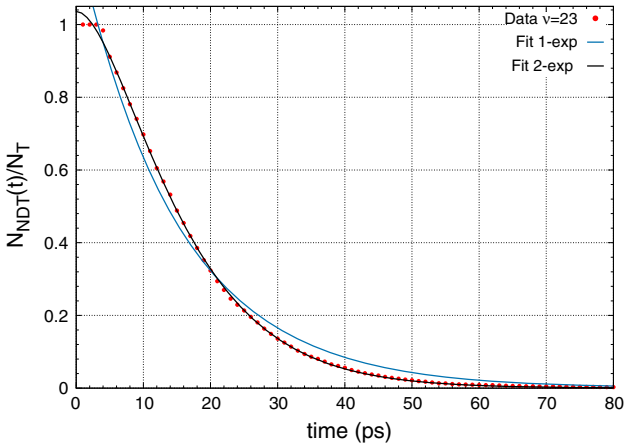

Fig. 3 QCTM population as a function of time for $v = 23$ and its fit using single [Eq. (22) or double [Eq. (23)] exponential law

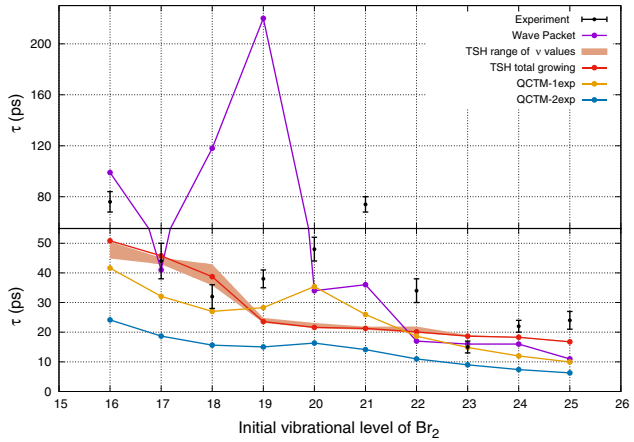

Fig. 4 Lifetimes for the TSH, QCTM, wave packets and experimental results, two last from Ref. [21]. The figure is divided in two parts to highlight the different time scales above and below 55 ps

because dissociating atoms have not yet reached the critical distance used as a dissociation criterion. These result in a non-exponential behavior. For this reason, lifetimes in the single exponential fit are larger than in the two exponential fit.

In the case of the TSH method, we use a multi-exponential law [16] to fit the obtained populations (see supplementary material):

$$N_p(t) = N_{p,\infty}(1 - e^{-bt})^c \tag{24}$$

where $N_p(t)$ is the vibrational population of the intermediate system at t and $N_{p,\infty}$ the asymptotic value of the fragments vibrational population. In this case, the lifetime is given by (see supplementary material):

$$\tau = -\frac{c}{b}\int_0^1 \ln(1-z)z^{c-1}\mathrm{d}z$$
$$z = (1 - e^{-bt}), \quad \mathrm{d}z = be^{-bt}\mathrm{d}t, \quad t = -\frac{1}{b}\ln(1-z). \tag{25}$$

The resulting lifetimes for each initial vibrational level v are plotted in Fig. 4, compared to the experimental product appearance times and to the wave packet results of Ref. [21]. For the TSH results, a range of values is represented, corresponding to the appearance time of Br_2 in each of the Δv exit channels, as well as the overall appearance time of Br_2 fragments (see Table 1 in supplementary material).

From v=16 to 18 there is a good agreement between the TSH and experimental results for the dissociation lifetimes. The most important difference among the lifetimes corresponds to the range $v = 19-22$, as was also observed in Ref. [21] between wave packet simulations and experiment. This is associated with the closure of the $\Delta v = -2$ channel. It occurs for $v = 19$ in the TSH method, and for $v = 20$ in the wave packet simulation, due to slight differences in the potential used. In both cases the closure is followed by a sudden decrease of the lifetime, although it is preceded by an erratic behavior in the wave packet simulations due to resonances in the sparse IVR regime (discussed below). These characteristics are not reproduced by the QCTM simulations since vibrational energy transfer is not quantified in this method and $\Delta v = -2$ only closes for $v = 24$. They exhibit a smooth decay of the dissociation lifetime with v, albeit with a small local maximum for $v = 20$. The single exponential fit of Eq. (22) for the QCTM results gives lifetimes closer to the results of the TSH and wave packet method ($v = 22 - 25$). This seems to indicate that the appearance time of the fragments is better fitted by depreciating the initial slow decay inherent to the use of classical dynamics.

On the other hand, the wave packet results obtained with the same interaction potentials as the QCTM results should be considered as the reference. However, in the $\Delta v = -2$ range ($v \leq 19$) where dissociation requires the transfer of only two vibrational quanta, the dynamics is typical of IVR in the sparse regime, where the initially excited ("bright") v level is coupled to one or very few "dark" levels in the $v - 1$ ensemble. As stated in Refs. [21,39], the rates are then very sensitive to the energy differences between the "bright" and "dark" levels. This effect is highly nonlinear and is strongly affected by the details of the potential (slight changes in the potential parameters strongly affect the dark level energies), the total angular momentum, as well as second-order effects such as the (small) mixing of the initial quasibound state of a given v level with the corresponding $v \pm 1$ quasibound states [39]. In particular, the lifetime for v=19 strongly depends on the total angular momentum J, as shown in Ref. [21], whereas they vary much less with J for $v = 21$. The simulations in Fig. 4 are performed for $J = 0$ whereas a large number of rotational levels are populated in the experiment, and the resonance effect is therefore smoothed out. This resonance effect is not reproduced in classical

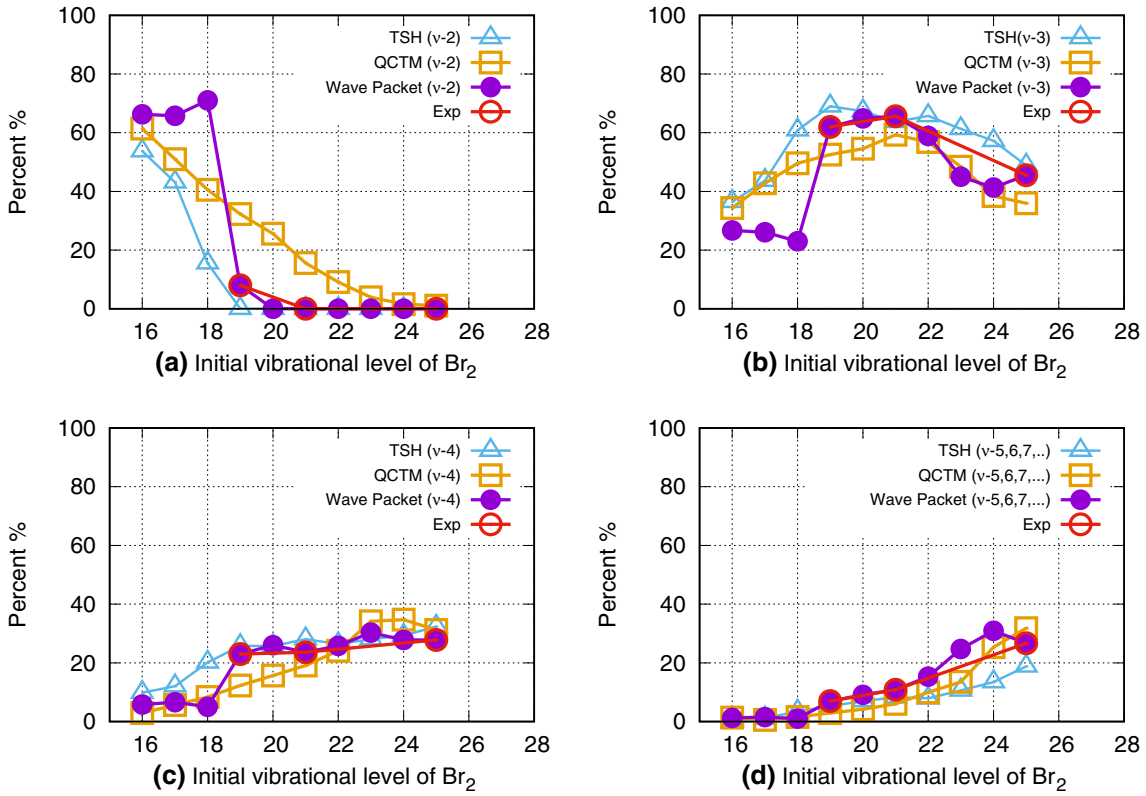

Fig. 5 Final vibrational state population (in %) of Br_2 as a function of initial vibrational level for the QCTM and the TSH method, compared to wavepacket simulation and experimental results from Ref. [21]. **a** $\Delta v = -2$ ($Br_2(v-2)$ products); **b** $\Delta v = -3$; **c** $\Delta v = -4$; **d** $\Delta v = -5$

dynamics; hence, the reason why classical results seem to be closer to experimental ones in the region of the closure of $\Delta v = -2$ is probably fortuitous.

For higher vibrational levels $v > 19$ where $\Delta v < -2$, the density of dark states is higher and IVR is in the intermediate regime where the lifetimes no longer oscillate. The TSH lifetimes show a sudden decrease at the closure of ($\Delta v = -2$), followed by a slower decrease with v. It does not show any resonant behavior. This is not really surprising since the intermolecular motion is described classically. However, given that the transfer of vibrational energy is quantized, the phase space accessible in $v - 2$ is very much reduced for $v = 19$ and this could favor quasi-periodic trajectories, hence a longer lifetime as in wavepacket results.

3.2 Fragments vibrational state distribution

In Fig. 5 we show the final vibrational state population of the Br_2 fragments as a function of initial v using the QCTM and TSH methods and compare with the results of wave packet simulations and of experiment from Ref. [21].

In the TSH case, $v = 19$ is closed for two vibrational quanta lost. The probabilities for hopping (vibrational transitions) are governed by the coupling terms $\langle v'| H_{int}(r, R, \theta)|v\rangle$, Eq. (21). As illustrated in Fig. 2b for $v = 20$, the strongest couplings correspond to $\Delta v = \pm 1$, which justifies considering only $\Delta v = -1$ steps in the kinetic mechanism discussed below.

For $v \geq 22$ the results for all methods used in this work are in rather good agreement with those previously reported. As can be seen in that figure, both methods reproduce reasonably well the experimental data. Nevertheless, the TSH method has the advantage in comparison to QCTM in that it does not need an approximate definition of the final state quantum numbers. In addition, the TSH method allows a description, from a kinetic point of view, of the path followed to dissociation.

3.3 Kinetic mechanism

The TSH populations have been fitted to the kinetic mechanism presented in the supplementary material in terms of the following elementary steps: IVR (intramolecular vibrational redistribution or IVR transfer of one vibrational quantum without dissociation), VP (transfer of one vibrational quantum inducing dissociation), or EC (evaporative cooling or dissociation of a warm intermediate complex without any vibrational quantum transfer).

Figure 6 shows the proportion of the paths ending with an EC step (IVR-EC) or a VP step (IVR-VP). As can be seen in that Figure, panel (a), the $\Delta v = -2$ channel is dominant among IVR-EC processes for $v =$

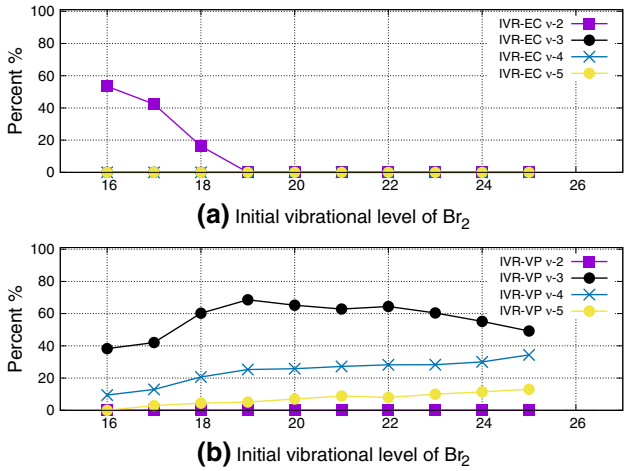

Fig. 6 Path followed (statistically) for each vibrational level. **a** IVR-EC and **b** IVR-VP process. Both panels correspond to $v-2,\ldots,5$

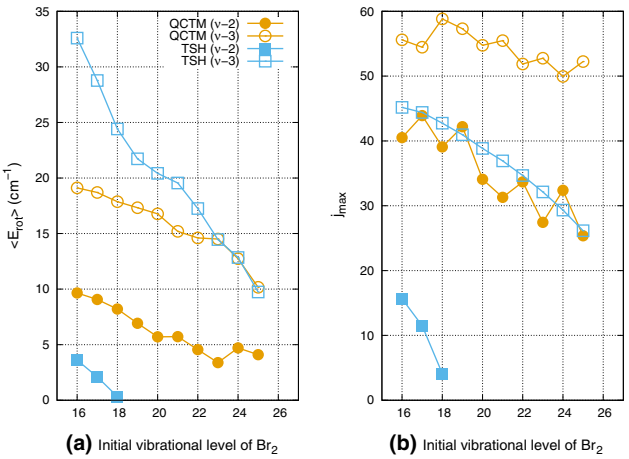

Fig. 7 QCTM and TSH results for **a** average rotational energy $\langle E_{rot}\rangle$ cm^{-1} and **b** the maximum angular momentum (j_{max}) reached in our simulations for Br_2 $\Delta v=-2,-3$

$16-18$ before closing, and the IVR-EC process does not occur for $v>18$ vibrational levels. Panel (b) shows that except for $v\leq 19$ the last step is always IVR-VP (contrary to what occurs upon transfer of the first vibrational quanta, the transfer of the last vibrational quantum does not lead to intramolecular vibrational redistribution but directly to dissociation).

For $16\leq v\leq 18$ IVR-VP competes with IVR-EC. However, IVR-EC is mostly for $\Delta v=-2$ and disappears for $v\geq 19$, whereas IVR-VP corresponds to $\Delta v=-3$, gradually shifting to -4 and then -5. IVR-EC $(v-2)$ can thus be attributed to the reduced phase space in $(\Delta v=-2)$ when this channel is open, which is the analogue of the sparse IVR regime of the wave packet study. IVR-VP with more than 2 vibrational quanta involved gradually wins over IVR-EC up to closure of the $\Delta v=-2$ channel. Among the IVR-VP channels, $\Delta v=-3$ (two $\Delta v=-1$ IVR steps followed by $\Delta v=-1$ IVR-VP) dominates, with a gradual increase of $\Delta v=-4$.

3.4 Rotational distribution of the Br_2 fragment

In Fig. 7 we compare the average rotational energy $\langle E_{rot}\rangle$ and the maximum angular momentum (j_{max}) for Br_2 using both methods employed in this work. In panel (a) we can observe that for TSH the system acquires lower average rotational energy than for QCTM (for two vibrational quanta energy lost). For three vibrational quanta lost, the behavior is reversed. This can be attributed to the continuous vibrational energy transfer in QCTM compared to its quantification in TSH. For Δv=-2, all the TSH trajectories have received exactly the same amount of energy from Br_2 vibration, $E^{B,v}_{Br_2}-E^{B,v-2}_{Br_2}$, whereas most of the QCTM trajectories have received more than that since Δv=-2 was barely open in the range considered ($v=16-18$) and $-\Delta v$ can be up to 2.5. For $\Delta v=-3$, the results tend to show that most of the QCTM trajectories receive less than that $E^{B,v}_{Br_2}-E^{B,v-3}_{Br_2}$ before dissociating. In panel (b) the maximum angular momentum (j_{max}) for Br_2 is higher using QCTM. This is again due to the continuous character of vibrational energy transfer in this method (the transfer of 2.49 quanta is collected in the Δv=-2 bin for instance). The difference is more important when the system loses two vibrational quanta of energy. Another difference between the methods originates from the PES taken into account. In the QCTM only one surface is involved, while for TSH the PES are slightly different for each vibrational level of the diatom v (see the top panel in Fig. 2).

A very convincing approach to improve final state distribution using QCTM is to implement Gaussian binning (GB), where trajectories are weighted following a Gaussian distribution rather than the standard binning used in this work. As recalled in Ref. 9, QCTM is very successful in reproducing final ro-vibrational state distributions except in the sparse IVR regime, in the vicinity of the closure of a vibrational channel. GB is shown to amend this shortcoming of the QCTM, at the expense of increasing by about one order of magnitude the number of trajectories required for convergence. It would be very instructive to perform a systematic comparison for $ArBr_2$. However, even in the GB version, QCTM is not able to describe the kinetics mechanism in terms of VP, IVR, and EC steps, since it is based on the kinetics of the vibrational quantum transfer which can only be directly identified in the TSH method.

In order to estimate the importance of the potential anisotropy, we have calculated the maximum theoretical value of j_{max} which is determined by energy conservation:

$$E_v+E_v^{vdWv}\geq E_{v'}+E_{v'}^{vdW}+\frac{\hbar^2 j(j+1)}{2\mu_{Br_2}}\langle v'|\frac{1}{r^2}|v'\rangle \tag{26}$$

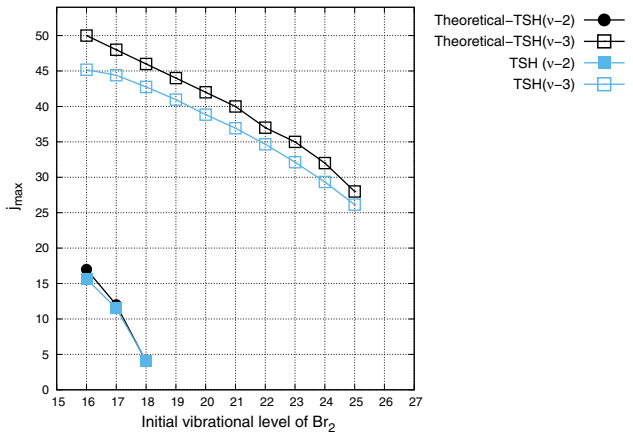

Fig. 8 Comparison of j_{max} between theoretical value obtained from energy conservation and the values obtained in our TSH simulation

In Fig. 8 we compare the theoretical j_{max} by using Eq. 26 with the results collected in Fig. 7b. The resulting maximum TSH values are close but not equal to the theoretical values. This shows that the potential anisotropy is important in the dissociation but not very strong.

4 Conclusions

We have investigated the vibrational predissociation process for the $ArBr_2$ system employing QCTM and TSH methods and obtained good results in comparison with previous work. In our simulations, we studied a range of vibrational levels from $v = 16$ to $v = 25$. We computed the lifetime, exit channel, average rotational energy, and maximum angular momentum (j_{max}) of Br_2.

We have shown that TSH in the diabatic representation provides a natural way of identifying the different paths leading to dissociation, thanks to the quantification of vibrational transfer in this mixed quantum-classical method. The results presented in Fig. 7 should be convenient for experimental verification of the theoretical analysis.

Acknowledgements - CCM acknowledges stimulating discussions at the UCI Liquid Theory Lunch (LTL) and the Telluride Science Research Center (TSRC) and support by the US National Science Foundation under grant CHE-1764209 - The authors would also like to thank Advanced Computational Team at Instituto Superior de Tecnologías y Ciencias Aplicadas (InSTEC) for the support provided during the realization of this work. - EGA, MMM, and JRS would like to thank NA223LH-INSTEC-003 project from InSTEC-UH. EGA thanks the Université Fédérale Toulouse Midi-Pyrénées for financial support through the "Chaires d'Attractivité 2014" Programme IMDYNHE.

Author contributions

All the authors were involved in the preparation of the manuscript and contributed equally to this work. All the authors have read and approved the final manuscript.

Data Availability Statement This manuscript has data included as electronic supplementary material.

References

1. O. Borrell-Grueiro, M. Márquez-Mijares, P. Pajón-Suárez, R. Hernández-Lamoneda, J. Rubayo-Soneira, Fragmentation dynamics of NO–NO dimer: a quasiclassical dynamics study. Chem. Phys. Lett. **563**, 20 (2013)
2. J. Rubayo-Soneira, A. Garcıía-Vela, G. Delgado-Barrio, P. Villarreal, Vibrational predissociation of I_2-Ne. A quasiclassical dynamical study. Hem. Phys. Lett. **243**, 236 (1995)
3. A. García-Vela, J. Rubayo-Soneira, G. Delgado-Barrio, P. Villarreal, Quasiclassical dynamics of the I_2-Ne_2 vibrational predissociation: a comparison with experiment. J. Chem. Phys. **104**, 8405 (1996)
4. O. Roncero, J. Campos-Martínez, M.I. Hernández, G. Delgado-Barrio, P. Villarreal, J. Rubayo-Soneira, Photodissociation of $NeBr_2$(B) below and above the dissociation limit of Br_2(B). J. Chem. Phys. **115**, 2566 (2001)
5. J.A. Cabrera, C.R. Bieler, B.C. Olbricht, W.E. Veer, K.C. Janda, Time-dependent pump-probe spectra of $NeBr_2$. J. Chem. Phys. **123**, 054311 (2005)
6. M.L. González-Martínez, J. Rubayo-Soneira, K. Janda, Quasi-classical trajectories study of $Ne^{79}Br_2(B)$ vibrational predissociation. Phys. Chem. Chem. Phys. **8**, 4550 (2006)
7. A. García-Vela, K.C. Janda, Quantum dynamics of $NeBr_2$ vibrational predissociation: the role of continuum resonances and doorway states. J. Chem. Phys. **124**, 034305 (2006)
8. J.I. Cline, D.D. Evard, B.P. Reid, N. Sivakumar, F. Thommen, K.C. Janda, Structure and dynamics of weakly bound molecular complexes. In: Weber, A. (Ed.) Reidel: Dordrecht, The Netherlands, pp. 533–551 (1987)
9. M.L. González-Martínez, W. Arbelo-González, J. Rubayo-Soneira, L. Bonnet, J.-C. Rayez, Vibrational predissociation of van der Waals complexes: quasi-classical results with Gaussian-weighted trajectories Chem. Phys. Lett. **463**, 65 (2008)
10. S.K. Reed, M.L. González-Martínez, J. Rubayo-Soneira, D.V. Shalashilin, Cartesian coupled coherence states simulations: Ne_nBr_2 dissociation as a test case. J. Chem. Phys. **134**, 054110 (2011)
11. O. Borrell-Grueiro, U. Baños-Rodrıíguez, M. Márquez-Mijares, J. Rubayo-Soneira, Vibrational predissociation dynamics of the nitric oxide dimer. Eur. Phys. J. D **72**, 121 (2018). https://doi.org/10.1140/epjd/e2018-90102-3
12. R. Prosmiti, C. Cunha, A.A. Buchachenko, G. Delgado-Barrio, P. Villarreal, Vibrational predissociation of $NeBr_2$(X, v=1) using an ab initio potential energy surface. J. Chem. Phys. **117**, 22 (2002)

13. B. Miguel, A. Bastida, J. Zúñiga, A. Requena, N. Halberstadt, Time evolution of reactants, intermediates, and products in the vibrational predissociation of $Br_2 \cdots Ne$: a theoretical study. J. Chem. Phys. **113**, 22 (2000)
14. T.A. Stephenson, N. Halberstadt, Quantum calculations on the vibrational predissociation of $NeBr_2$: evidence for continuum resonances. J. Chem. Phys. **112**, 5 (2000)
15. A. Bastida, J. Zúñiga, A. Requena, I. Sola, N. Halberstadt, J.A. Beswick, Application of trajectory surface hopping to vibrational predissociation. Chem. Phys. Lett. **280**, 185 (1997)
16. A. Bastida, J. Zúñiga, A. Requena, N. Halberstadt, J.A. Beswick, Vibrational predissociation dynamics of $I_2 \cdots Ne_2$: a trajectory surface hopping study. J. Chem. Phys. **109**, 6320 (1998)
17. S. Fernandez Alberti, N. Halberstadt, J.A. Beswick, A. Bastida, J. Zúñiga, A. Requena, Intramolecular vibrational redistribution and fragmentation dynamics of $I_2 \cdots Ne{-}n$ clusters. J. Chem. Phys. **111**, 239 (1999)
18. A. Bastida, B. Miguel, J. Zúñiga, A. Requena, I. Sola, N. Halberstadt, K.C. Janda, Hybrid quantum/classical simulation and kinetic study of the vibrational predissociation of $Cl_2 \cdots Ne_n$ ($n = 2, 3$). J. Chem. Phys. **111**, 4577 (1999)
19. A. Rohrbacher, N. Halberstadt, K.C. Janda, The dynamics of noble gas-halogen molecules and clusters. Ann. Rev. Phys. Chem. **51**, 405 (2000)
20. R. Prosmiti, C. Cunha, P. Villarreal, G. Delgado-Barrio, Ab initio ground state potential energy surfaces for Rg–Br_2, (Rg=He, Ne, Ar) complexes. J. Chem. Phys. **116**, 21 (2002)
21. J. Cabrera, C.R. Bieler, N. McKinney, W.E. van der Veer, J.M. Pio, O. Roncero, K. Janda, Time and frequency resolved dynamics of $ArBr_2$. J. Chem. Phys. **127**, 164309 (2007)
22. J.C. Acosta-Matos, L. Uranga-Piña, Trajectory-based modeling of the quantum dynamics of vibrational predissociation: application to the $Ar\ldots Br_2(\nu = 24)$ complex. J. Chem. Phys. **529**, 110554 (2020)
23. J.M. Pio, W.E. van der Veer, C.R. Bieler, K.C. Janda, Product state resolved excitation spectroscopy of He, Ne, and Ar–Br_2 linear isomers: experiment and theory. J. Chem. Phys. **128**, 134311 (2008)
24. J.C. Tully, Molecular dynamics with electronic transitions. J. Chem. Phys. **93**, 1061 (1990)
25. E. García-Alfonso, M. Márquez-Mijares, J. Rubayo-Soneira, N. Halberstadt, K.C. Janda, C.C. Martens, Study of the vibrational predissociation of the $NeBr_2$ complex by computational simulation using the trajectory surface hopping method. Sigma Math. **8**, 2029 (2020)
26. A. Rodríguez-Fernández, M. Márquez-Mijares, J. Rubayo-Soneira, A. Zanchet, A. García-Vela, L. Bañares, Trajectory surface hopping study of the photodissociation dynamics of methyl radical from the 3s and $3p_z$ Rydberg states. Chem. Phys. Lett. **712**, 171–176 (2018)
27. A. Rodríguez-Fernández, M. Márquez-Mijares, J. Rubayo-Soneira, A. Zanchet, L. Bañares, Quasi-classical study of the photodissociation dynamics of the methyl radical. Rev. Cuba. Fis. **34**, 41 (2017)
28. C.C. Martens, Communication: fully coherent quantum state hopping. J. Chem. Phys. **143**, 141101 (2015)
29. A. Bastida, J. Zúñiga, A. Requena, N. Halberstadt, J.A. Beswick, Competition between electronic and vibrational predissociation in Ar-I_2 (B): a molecular dynamics with quantum transitions study. Chem. Phys. **240**, 229–239 (1999)
30. R. Barrow, T. Clark, J. Coxon, K. Yee, J. Mol. Spectrosc. **51**, 428 (1974)
31. A. Alexei, B. Alexei, Yu. Baisogolov and Nikolai, F. Stepanov, Interaction potentials and fragmentation dynamics of the Ne–Br_2, complex in the ground and electronically excited States. J. Chem. Soc. Faraday Trans. **90**, 3229–3236 (1994)
32. S. Nangia, A.W. Jasper, T.F. Miller, D.G. Truhlar, Army ants algorithm for rare event sampling of delocalized nonadiabatic transitions by trajectory surface hopping and the estimation of sampling errors by the bootstrap method. J. Chem. Phys. **120**, 3586 (2004)
33. J.E. Subotnik, W. Ouyang, B.R. Landry, Can we derive Tullys surface-hopping algorithm from the semiclassical quantum Liouville equation? Almost, but only with decoherence. J. Chem. Phys. **139**, 214107 (2013)
34. A.A. Buchachenko, A.Y. Baisogolov, N.F. Stepanov, Interaction potentials and fragmentation dynamics of the Ne–Br_2 complex in the ground and electronically excited States. J. Chem. Soc. Faraday Trans. **90**, 3229–3236 (1994)
35. R.L. Burden, J.D. Faires, *Numerical Analysis*, 9th ed.; Julet, M., Ed.; Brooks/Cole Cengage Learning: Boston, MA 02210 USA; pp. 173–259 (2010)
36. R. Crespo-Otero, M. Barbatti, Recent advances and perspectives on nonadiabatic mixed quantum-classical dynamics. Chem. Rev. Am. Chem. Soc. **118**, 7026 (2018)
37. A.W. Jasper, S.N. Stechmann, D.G. Truhlar, Fewest-switches with time uncertainty: a modified trajectory surface-hopping algorithm with better accuracy for classically forbidden electronic transitions. J. Chem. Phys. **116**, 3 (2002)
38. A.W. Jasper, D.G. Truhlar, Improved treatment of momentum at classically forbidden electronic transitions in trajectory surface hopping calculations. Chem. Phys. Lett. **369**, 60–67 (2003)
39. N. Halberstadt, J.A. Beswick, O. Roncero, K.C. Janda, Intramolecular vibrational relaxation in a triatomic Van der Waals molecule: $Ar\cdots Cl_2$. J. Chem. Phys. **96**, 2404 (1992)